Optimum holographic elements recorded with nonspherical wave fronts

K. A. Winick* and J. R. Fienup

Environmental Research Institute of Michigan, P.O. Box 8618, Ann Arbor, Michigan 48107

Received June 22, 1982

The problem of designing a flat, aspheric, holographic optical element that images a finite set of input wave fronts into a finite set of output wave fronts is rigorously analyzed. The optimum phase transfer function of the holographic optical element is analytically determined. The optimum phase transfer function is defined as the one for which the element has minimum mean-squared wave-front error averaged over the set of input wave fronts. It is also shown that in general it may not be possible to obtain a low value for this average mean-squared wave-front error by using a single holographic element. Furthermore, the performance trade-off of spherical aberration, coma, and astigmatism versus geometric distortion is clearly indicated by example.

1. INTRODUCTION

An optical system can be thought of as a device that transforms input wave fronts into output wave fronts. A simple glass lens is an example of such a system. Today most optical systems are composed of refractive (lenses) and reflective (mirrors) elements, and these systems are used primarily for imaging. The class of transformations that link the output wave fronts to the input wave fronts in refractive–reflective optical systems is quite limited. For example, it is not possible to design a refractive–reflective optical system for which the output wave front is a three-dimensional image of a teapot when the input wave front is a collimated beam. This particular input–output transformation can, however, be realized by using a hologram. Holograms can also be made to have transfer functions that are desirable in optical systems, in which case they are referred to as holographic optical elements (HOE's).[1] We note that the optical transfer function of a HOE is based on diffraction phenomena, and therefore the characteristics of these elements will be highly wavelength dependent. Consequently, HOE's are useful and sometimes indispensible components of optical systems when the source is monochromatic or when a wavelength-dependent system is desired.

Given an arbitrary input wave front, a HOE can, in principle, be designed to transform this input wave front into an arbitrary output wave front. In such a situation, the required HOE recording beams would most likely be produced by computer-generated holograms[2] in conjunction with conventional refractive and reflective optical elements.

It is natural to characterize a HOE by its phase transfer function. Since a conventional optical element, such as a glass lens, cannot be similarly characterized unless it is physically thin, the design approach described in this paper is not immediately applicable to conventional optical design.

Most applications require optical systems that transform a set of input wave fronts into another set of output wave fronts rather than just one input wave front into just one output wave front. For example, a Fourier-transform lens, whether it be conventional or holographic, should map each input plane-wave spatial frequency into a single unaberrated point focus in the back focal plane of the lens.[3] Furthermore, in the back focal plane the (x, y) coordinates of a point focus and the corresponding input spatial frequency (f_x, f_y) should be linearly related according to $x = \lambda F f_x$ and $f = \lambda F f_y$, where λ is the wavelength and F is the focal length of the lens. It is well known that a Fourier-transform HOE, recorded using a single collimated beam and a single spherical converging beam, will form an unaberrated point focus at the proper location in the transform plane only for the single spatial frequency corresponding to that of the collimated recording beam. At other spatial frequencies (or equivalently at other input field angles), the point focus is aberrated and improperly located.[4,5] In order to define performance quantitatively, it is reasonable to consider some finite set of spatial frequencies and to compute at each of these the wave-front error of the Fourier-transform HOE. This wave-front error is the mean-squared deviation of the actual output wave front at the back of the HOE from the desired wave front. The wave-front errors for all the spatial frequencies can then be averaged to arrive at a measure of the HOE's performance. It has been demonstrated that a Fourier-transform HOE can be produced that has a smaller average mean-squared wave-front error over some set of field angles than the simple HOE described above.[6] This higher-performance Fourier-transform HOE is recorded by using more-complicated wave fronts than simple collimated and spherical beams.

HOE's produced by nonspherical recording beams (a collimated beam is considered to be a spherical beam of infinite radius of curvature) have been named aspheric HOE's.[6] The substrates on which aspheric HOE's are recorded may be either flat or curved.

To date, the procedure outlined below has been used to design optical systems that contain HOE's.[6] A merit function is specified that assigns a numerical value to the "goodness" of the system. The merit function can include any measure of the system performance, such as spot size, aberrations, and ray efficiencies. The value of the merit function is nonnegative. It is zero for a perfect optical system and increases as the performance departs from the ideal. The optical system

Reprinted from **Journal of the Optical Society of America,** Vol. 73, page 208, February 1983.

is defined up to a finite number of unknown parameters. These unknown parameters typically specify such things as the spacing between elements and the surface curvatures of elements. The phases of both of the two recording-beam wave fronts of the HOE determine the transfer function of the HOE and are described by analytic expressions that also contain unspecified parameters. These analytic expressions are often polynomials having unspecified coefficients. Slow spatial variations of the amplitude of a recording beam do not appreciably affect the aberration properties of the HOE, and so, for simplicity, the wave-front amplitudes are assumed to be constant. The numerical value of the merit function is evaluated by using a ray-tracing computer program, such as the holographic optics analysis and design (HOAD) program.[7,8] Using computer-implemented iterative optimization techniques, such as damped least squares,[9] in conjunction with a ray-tracing program, one attempts to determine the unspecified parameters of the system that will minimize the merit function. Once these parameters are found, the HOE recording beams are known, and optical systems must be devised for producing them. The systems for forming the recording beams will most likely consist of computer-generated holograms (CGH's) in conjunction with conventional refractive and reflective optics. CGH's would usually be required because of the nonspherical, nonrotationally symmetric, arbitrary functional form of the recording beams. Conventional optics would also usually be required in the recording systems both to allow for a spatial-filtering stage (to filter out unwanted orders of diffraction from the CGH) and to provide the lower-order terms, such as tilt, focus, and astigmatism, that would require finer fringe frequencies than that which the CGH recording device can supply.

We suggest that the following alternative two-level design approach may be useful in some cases. Instead of updating all the system parameters, including the HOE parameters, at the same time at each iteration, one could do an optimization of the HOE parameter for every update of the remaining system parameters. This would be desirable since a HOE can have many parameters, although it operates in only a single surface of the optical system. In order to optimize the HOE, it would first be necessary to do both forward and backward ray traces through the two halves of the optical system up to the surface of the HOE. The forward ray traces define the wave fronts incident upon the HOE. The backward ray traces, starting with ideal wave fronts in the back pupil of the optical system, define the wave fronts that would ideally be transmitted by the HOE. The problem of optimizing the HOE is to find the parameters of the HOE that come closest to transforming the given incident wave fronts into the respective ideal transmitted wave fronts. The optimization of the HOE parameters could employ the same types of techniques described earlier for the optical system.

The design approaches described above, despite their power and generality, do not necessarily arrive at the optimal solution. That is, the procedure may not find the recording wave fronts for the HOE that absolutely minimize the merit function. This is a consequence of two factors. The first factor is that the technique can consider only a subset of all possible recording-beam wave fronts, limited by the kind and number of parameters available. Clearly, one could include enough parameters to account for all useful variations of recording-beam wave fronts. The number of parameters, however, might be extremely large, and optimization of so many parameters would not be practical. The second factor is that optimization routines are essentially trial-and-error procedures, and there is no guarantee that such procedures will find the best solution among some set of possible solutions, particularly if there exist local minima of the merit function.

In the remainder of this paper we propose and analyze another approach to the optimization of the HOE that does not depend on a finite number of parameters. We assume that the HOE is part of an optical system that is completely specified (known) except for the HOE. By this new method the HOE recording wave fronts are found that minimize a HOE merit function absolutely. The HOE merit function in question is a weighted mean-squared wave-front error, which is attractive because it relates directly to a physically meaningful quantity, the Strehl ratio,[10] and correlates well with the rms spot sizes for the case of imaging. As an example, we apply the method to the design of a HOE for use as a Fourier-transform lens.

2. PROBLEM STATEMENT

Suppose that we have a set of N incoming wave fronts specified by a description of their phases $\phi_{n,\text{in}}(x, y)$ at the HOE. The surface of the HOE lies in the x–y plane. For a flat HOE, the relationship between the phase $\phi_{n,\text{in}}(x, y)$ of an incoming wave front at the HOE and the phase $\phi_{n,\text{out}}(x, y)$ of the corresponding output wave front at the HOE is given by

$$\phi_{n,\text{out}}(x, y) = \phi_{n,\text{in}}(x, y) + \phi_H(x, y), \tag{1}$$

where $\phi_H(x, y)$, the phase transfer function of the HOE, is given by

$$\phi_H(x, y) = \phi_{\text{obj}}(x, y) - \phi_{\text{ref}}(x, y) \tag{2}$$

and where $\phi_{\text{ref}}(x, y)$ and $\phi_{\text{obj}}(x, y)$ are the phases at the element of the reference and object beams, respectively, with which the HOE was recorded. For each of these input wave fronts, we specify the phase $\phi_n(x, y)$ at the HOE that corresponds to some desired output wave front. The problem then is to determine the phase transfer function of the HOE, $\phi_H(x, y)$, so that the mean-squared wave-front error [the squared deviation of $\phi_{n,\text{out}}(x, y)$ from $\phi_n(x, y)$] averaged over the set of N output wave fronts is minimum.

We define the weighted mean-squared wave-front error E^2 by

$$E^2 = \eta \sum_{n=1}^{N} W_n \iint P_n(x, y)\,[\phi_{n,out}(x, y) - \phi_n(x, y)]^2 \mathrm{d}x\mathrm{d}y, \tag{3a}$$

where $P_n(x, y)$ is a function that has a value of 1 for all points (x, y) on the hologram illuminated by the nth input wave-front and has a value of 0 elsewhere. W_n is the weight given to the nth wave front, and η is the normalizing factor:

$$\eta = \frac{1}{4\pi^2}\left[\sum_{n=1}^{N} W_n \iint P_n(x, y)\mathrm{d}x\mathrm{d}y\right]^{-1}. \tag{3b}$$

The square root of this quantity, E, is the rms wave-front error. The problem then is to determine $\phi_H(x, y)$ so that E is minimum. The region of the integration in Eqs. (3) and in all remaining equations in this paper is the entire x–y plane.

3. THE OPTIMAL SOLUTION: A NAIVE APPROACH

Equations (1) and (3) can be combined to yield

$$E^2 = \eta \sum_{n=1}^{N} W_n \iint P_n(x,y)\,[\phi_H(x,y) - \phi_{H,n}(x,y)]^2 dx\,dy, \tag{4}$$

where

$$\phi_{H,n}(x,y) \triangleq \phi_n(x,y) - \phi_{n,\text{in}}(x,y) \tag{5}$$

is the phase transfer function of the HOE that would be optimum for the nth wave front. Equation (4) can be rewritten as

$$E^2 = \eta \iint \sum_{n=1}^{N} W_n P_n(x,y)\,[\phi_H(x,y) - \phi_{H,n}(x,y)]^2 dx\,dy. \tag{6}$$

It is clear from Eq. (6) that in order to minimize E it is sufficient to choose $\phi_H(x,y)$ such that

$$e^2(x,y) \triangleq \eta \sum_{n=1}^{N} W_n P_n(x,y)\,[\phi_H(x,y) - \phi_{H,n}(x,y)]^2 dx\,dy \tag{7}$$

is minimum for all points (x,y). Now arbitrarily pick some point (x,y). Then $\phi_{H,n}(x,y)$, $n = 1, \ldots, N$ are known constants and $\phi_H(x,y)$ is an unknown constant. We wish to determine $\phi_H(x,y)$ so that $e^2(x,y)$ is minimum. This $\phi_H(x,y)$ can be found by differentiating $e^2(x,y)$ with respect to $\phi_H(x,y)$ and setting the derivative to zero. When this is done, it immediately follows that $e^2(x,y)$ is the minimum if

$$\phi_H(x,y) = \left[\sum_{n=1}^{N} W_n P_n(x,y)\right]^{-1} \sum_{n=1}^{N} W_n P_n\,(x,y)\phi_{H,n}(x,y). \tag{8}$$

But point (x,y) was arbitrarily chosen, and so $e^2(x,y)$ is minimum for all points (x,y), and therefore E is minimum if $\phi_H(x,y)$ is given by Eq. (8) above. Thus the optimum phase is just the weighted average of the phases that are optimum for the N individual wave fronts.

Although Eq. (8) is exact, it is naive in the sense that it assumes that one knows the desired output wave front ϕ_n, used in Eq. (5) to compute $\phi_{H,n}$, in complete detail. As will be shown in Section 4, by allowing a different constant additive phase to be associated with each ϕ_n, and by optimizing over the values of those constant phases, one can arrive at a HOE having improved performance. Furthermore, as will be brought out in Sections 6 and 7, allowing additional degrees of freedom in the output wave fronts by ignoring certain aberrations makes it possible to reduce all the other aberrations to a greater degree.

4. THE OPTIMAL SOLUTION REVISITED

Below we investigate this result more critically. We note that when imaging is to be performed the concept of absolute phase of a wave front is not useful. For example, expressions (9) and (10) below both describe a perfect spherical wave converging to the point (x_s, y_s, z_s):

$$\exp\left\{-i\,\frac{2\pi}{\lambda}\,[(x-x_s)^2 + (y-y_s)^2 + (z-z_s)^2]^{1/2}\right\}, \tag{9}$$

$$\exp\left\{-i\,\frac{2\pi}{\lambda}\,[(x-x_s)^2 + (y-y_s)^2 + (z-z_s)^2]^{1/2} + i\gamma\right\} \tag{10}$$

(γ is a real constant). The absolute phases of these two wave fronts differ by the constant γ, although the images of the two wave fronts are identical. Let us use the notation developed earlier and specify the desired phase of the first output wave front by

$$\phi_1(x,y) = \frac{-2\pi}{\lambda}\,[(x-x_s)^2 + (y-y_s)^2 + z_0^2]^{1/2} \tag{11}$$

at the plane $z - z_s = z_0$. Now if the actual phase of the output wave front as given by expression (10) is

$$\phi_{1,\text{out}}(x,y) = \frac{-2\pi}{\lambda}\,[(x-x_s)^2 + (y-y_s)^2 + z_0^2]^{1/2} + \gamma, \tag{12}$$

we should conclude that the wave-front error is zero since the images are identical. According to Eq. (3), however, the wave-front error E_1 for this first output wave front is given by

$$\begin{aligned} E_1^2 &= W_1 \iint P_1(x,y) \times [\phi_{1,\text{out}}(x,y) - \phi_1(x,y)]^2 dx\,dy \\ &= W_1 \iint P_1(x,y)\gamma^2 dx\,dy > 0. \end{aligned} \tag{13}$$

This problem arises because the definition of wave-front error as given by Eq. (3) is not consistent with the physics of the situation. A better definition of wavefront error *for imaging applications* is

$$E^2 \triangleq \eta \sum_{n=1}^{N} W_n \iint P_n(x,y) \times [\phi_{n,\text{out}}(x,y) - \phi_n(x,y) + \gamma_n]^2 dx\,dy, \tag{14}$$

where γ_n, $n = 1, \ldots, N$ is a set of real numbers chosen to remove any absolute phase difference between $\phi_{n,\text{out}}(x,y)$ and $\phi_n(x,y)$. This is equivalent to saying that, for a specified $\phi_{n,\text{out}}(x,y)$ and $\phi_n(x,y)$, $n = 1, \ldots, N$, the γ_n's should be chosen so that E is minimum. Then the mean-squared wave-front error will be

$$E^2 \triangleq \eta \min G(\gamma_1, \gamma_2, \ldots, \gamma_N), \tag{15}$$

where

$$G(\gamma_1, \gamma_2, \ldots, \gamma_N) = \iint \sum_{n=1}^{N} W_n P_n(x,y) \times [\phi_{n,\text{out}}(x,y) - \phi_n(x,y) + \gamma_n]^2 dx\,dy. \tag{16}$$

Note that the specified absolute phase of any output wave-front $\phi_n(x,y)$ is now meaningless since changes in absolute phase are not observable and will not affect the value of the wave-front error as defined by Eqs. (15) and (16). Similarly, it is easy to see that the absolute phase assigned to any input wave front is also without meaning.

Combining Eqs. (1) and (5), we have

$$\phi_{n,\text{out}}(x,y) - \phi_n(x,y) = \phi_H(x,y) - \phi_{H,n}(x,y). \tag{17}$$

By using Eq. (17), Eq. (16) becomes

$$G(\gamma_1, \gamma_2, \ldots, \gamma_N) = \sum_{n=1}^{N} W_n \iint P_n(x, y) \times \{\phi_H(x, y) - [\phi_{H,n}(x, y) - \gamma_n]\}^2 dx\,dy. \quad (18)$$

Using the same argument that led to Eq. (8), it is easy to see that, for fixed but arbitrary γ_n's, $G(\gamma_1, \gamma_2, \ldots, \gamma_N)$ will be minimum if

$$\phi_H(x, y) = \left[\sum_{m=1}^{N} W_m P_m(x, y)\right]^{-1} \sum_{m=1}^{N} W_m P_m(x, y) \times [\phi_{H,m}(x, y) - \gamma_m]. \quad (19)$$

Thus the HOE phase $\phi_H(x, y)$ should be chosen according to Eq. (19). Inserting Eq. (19) into Eq. (18), expanding, and then combining terms, one gets

$$G(\gamma_1, \gamma_2, \ldots, \gamma_N) = \iint \Bigg(\sum_{n=1}^{N} W_n P_n(x, y)\,[\phi_{H,n}(x, y) - \gamma_n]^2 - \left[\sum_{s=1}^{N} W_s P_s(x, y)\right]^{-1} \times \left\{\sum_{r=1}^{N} W_r P_r(x, y)[\phi_{H,r}(x, y) - \gamma_r]\right\}^2 \Bigg) dx\,dy. \quad (20)$$

Now, by Eqs. (15) and (16), the mean-squared wave-front error is given by η times the minimum of $G(\gamma_1, \gamma_2, \ldots, \gamma_N)$. If we can find $\gamma_1 = \hat{\gamma}_1, \gamma_2 = \hat{\gamma}_2, \ldots, \gamma_N = \hat{\gamma}_N$ such that $G(\gamma_1, \gamma_2, \ldots, \gamma_N)$ is minimum, then Eq. (19) will define the phase transfer function of the HOE that results in the minimum mean-squared wave-front error. Our goal now is to determine $\hat{\gamma}_1, \hat{\gamma}_2, \ldots, \hat{\gamma}_N$. Note that [see Eq. (18)]

$$G(\gamma_1, \gamma_2, \ldots, \gamma_N) \geq 0. \quad (21)$$

Equation (20) can be rewritten as

$$G(\gamma_1, \gamma_2, \ldots, \gamma_N) = c + \sum_{n=1}^{N} a_n \gamma_n + \sum_{j=1}^{N} \sum_{k=1}^{N} b_{jk} \gamma_j \gamma_k, \quad (22)$$

where the a_n's, b_{jk}'s, and c are real constants (see Appendix A). It can be shown that the γ_n's that minimize $G(\gamma_1, \gamma_2, \ldots, \gamma_N)$ are the solutions of the N equations in N unknowns given below:

$$0 = \frac{\partial G}{\partial \gamma_p} = a_p + 2 \sum_{j=1}^{N} b_{pj} \gamma_j, \qquad p = 1, 2, \ldots, N. \quad (23)$$

(Note from Appendix A that $b_{jk} = b_{kj}$.) Furthermore, it can be shown that, if $\gamma_1 = \hat{\gamma}_1, \gamma_2 = \hat{\gamma}_2, \ldots, \gamma_N = \hat{\gamma}_N$ is a solution of Eqs. (23), then all solutions of Eqs. (23) are of the form $\gamma_1 = \hat{\gamma}_1 + \omega, \gamma_2 = \hat{\gamma}_2 + \omega, \ldots, \gamma_N = \hat{\gamma}_N + \omega$, where ω is a constant. All these solutions are equally good and result in optimum HOE transfer functions that differ only by a constant [see Eq. (19)].

To summarize, suppose that we have a set of N incoming wave fronts, the nth one having phase $\phi_{n,\text{in}}(x, y)$ at the HOE. For each of these wave fronts, we specify the phase $\phi_n(x, y)$ of the corresponding desired output wave front. The actual phase of the nth output wave front is

$$\phi_{n,\text{out}}(x, y) = \phi_{n,\text{in}}(x, y) + \phi_H(x, y),$$

where $\phi_H(x, y)$ is the phase transfer function of the HOE. Then the optimum $\phi_H(x, y)$, i.e., the $\phi_H(x, y)$ that minimizes the weighted mean-squared difference between $\phi_{n,\text{out}}(x, y)$ and $\phi_n(x, y)$ averaged over the set of N incoming wave fronts ($n = 1, \ldots, N$), is given by Eq. (19), where the γ_n's are a solution of Eqs. (23).

5. RAY TRACING AND SPOT SIZE

A discussion of the ray-trace grating equations and spot size is appropriate at this point. We assume that a flat HOE is recorded with an object beam (obj) and a reference beam (ref) having phases $\phi_{\text{obj}}(x, y)$ and $\phi_{\text{ref}}(x, y)$, respectively, at the surface of the HOE. The phase transfer function $\phi_H(x, y)$ of the HOE is then given by Eq. (2). During a ray trace through the HOE, an input ray (in) having phase $\phi_{\text{in}}(x, y)$ impinges upon the hologram at the coordinate (x, y) and is diffracted by the hologram, resulting in an output ray (out). The phase $\phi_{\text{out}}(x, y)$ and the x, y, z direction cosines $l(x, y)$, $m(x, y)$, and $n(x, y)$, respectively, of the output ray are given by the grating equations

$$\phi_{\text{out}}(x, y) = \phi_{\text{in}}(x, y) + \phi_H(x, y), \quad (24a)$$

$$l_{\text{out}}(x, y) = l_{\text{in}}(x, y) + \frac{\lambda}{2\pi} \frac{\partial \phi_H(x, y)}{\partial x}, \quad (24b)$$

$$m_{\text{out}}(x, y) = m_{\text{in}}(x, y) + \frac{\lambda}{2\pi} \frac{\partial \phi_H(x, y)}{\partial y}, \quad (24c)$$

$$n_{\text{out}}(x, y) = \pm[1 - l_{\text{out}}^2(x, y) - m_{\text{out}}^2(x, y)]^{1/2}, \quad (24d)$$

where λ is the input-ray wavelength. The sign choice in Eq. (24d) is used to select either the $-z$ direction of propagation of the diffracted wave front or the $+z$ direction of propagation. In Fig. 1, the $-z$ direction corresponds to transmission, whereas the $+z$ direction corresponds to reflection. The ray-intercept coordinates of an output ray at an arbitrary plane are determined by the ray's x, y, z direction cosines as given by Eqs. (24b)–(24d). If $l_{\text{out}}^2(x, y) + m_{\text{out}}^2(x, y) > 1$, then the output ray is evanescent and will fail to propagate away from the HOE.

Note that

$$\frac{\partial \phi_H(x, y)}{\partial x}, \qquad \frac{\partial \phi_H(x, y)}{\partial y}$$

do not exist at all (x, y) since $\phi_H(x, y)$, as given by Eq. (19), is only piecewise continuous. $\phi_H(x, y)$ would be continuous and have first partial derivatives everywhere, however, if $P_1(x, y)$, $P_2(x, y), \ldots, P_N(x, y)$ were continuous and had first

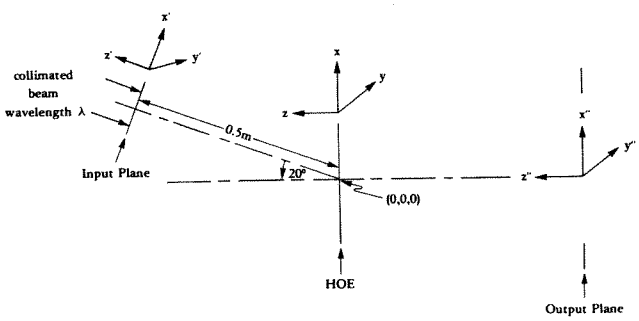

Fig. 1. Fourier-transform HOE geometry.

partial derivatives everywhere. As it is, $P_n(x, y)$ is continuous and has first partial derivatives everywhere except at its boundaries, i.e., at the transition between $P_n(x, y) = 0$ and $P_n(x, y) = 1$. The set of all points S that are boundary points of the $P_n(x, y)$'s occupy zero area of the HOE. Thus we can neglect these points since they do not contribute to the integral given in Eq. (14).

By Eq. (19), using the fact that $P_m(x, y)$ is piecewise constant,

$$\frac{\partial \phi_H(x, y)}{\partial x} = \left[\sum_{m=1}^{N} W_m P_m(x, y)\right]^{-1} \times \sum_{m=1}^{N} W_m P_m(x, y) \frac{\partial \phi_{H,m}(x, y)}{\partial x} \quad (25)$$

for $(x, y) \notin S$, and similarly for the partial derivative with respect to y. Therefore the ray-intercept coordinate of an output ray on any arbitrarily chosen plane will be independent of the γ_n's. Since ray-trace spot size is the size of the region occupied by a set of ray intercepts, it also is independent of the γ_n's. The relationship between observed spot size and ray-trace-predicted size is discussed below.

Ray-tracing techniques do not take into account boundary diffraction effects and can therefore give inaccurate results when such effects are significant. Boundary diffraction effects will result in observed spot sizes larger than those predicted by ray-tracing methods. If we consider a single HOE, there are two principal sources of boundary effects. The first is the finite size of the HOE, and the second is discontinuities of the phase transfer function. Diffraction effects that are due to the finite size of the HOE are easily evaluated. For instance, a Fourier-transform HOE of diameter D and focal length F, with a continuous phase transfer function, has a diffraction-limited spot size of $1.22\lambda F/D$.[3] If a ray trace through this HOE predicts a spot size considerably smaller than $1.22\lambda F/D$, then the observed spot size will be nominally $1.22\lambda F/D$. If the ray trace predicts a spot size larger than $1.22\lambda F/D$ then the actual experimentally observed spot size will be nominally the same as that indicated by the ray trace. In the remainder of this discussion we neglect effects that are due to the finite size of the HOE. Diffraction effects arising from discontinuities of the HOE's phase transfer function are more difficult to evaluate. They will depend on the number of discontinuities, their locations, and their magnitudes. Large discontinuities will likely result in large values of the rms wave-front error E, as given by Eqs. (15) and (16). Since E does not contain all the information regarding the discontinuities (i.e., the number of discontinuities, their locations, and their magnitudes), a direct correlation between observed spot size and E does not necessarily exist for large values of E. As a consequence, the technique outlined in this paper should be used with care in situations in which a HOE having a reasonably small rms wave-front error does not exist. For situations in which a HOE having a reasonably small rms wave-front error does exist, the technique outlined in Section 4 will result in an optimum design.

Recall that the γ_n's can significantly affect the rms wave-front error. This is because the γ_n's strongly influence the magnitude of the discontinuities of the phase function. The boundaries of the P_n's determine the locations of the discontinuities. These discontinuities can result in large rms wave-front errors, even in the presence of small spot sizes predicted by ray-tracing methods. A careful examination of diffraction effects would indicate that small values of E imply small observed spot sizes and vice versa. Furthermore, small E or small ray-trace-predicted spot sizes imply together with Eqs. (15) and (18) that

$$\phi_{H,l}(x, y) \simeq \phi_{H,m}(x, y) + c_{lm} \quad (26)$$

for all l and m in the region where

$$P_l(x, y)P_m(x, y) = 1$$

(c_{lm} is a constant). Formula (26) asserts that the desired phase transfer functions corresponding to the input wave fronts are nearly identical up to an additive constant in the regions where they overlap. It is easy to see that if formula (26) is satisfied then E will be minimum, provided that γ_l and γ_m are chosen such that $\gamma_l - \gamma_m = c_{lm}$. Furthermore, in such a case, the minimum value of E will be small. Choosing $\gamma_l - \gamma_m = c_{lm}$ tends to minimize the magnitude of the discontinuities of the phase transfer function $\phi_H(x, y)$. In summary,

1. A small value of E indicates small observed spot sizes and vice versa.
2. Observed spot sizes are larger than ray-trace-predicted spot sizes.
3. Ray-trace-predicted spot sizes are independent of the γ_n's. Small ray-trace-predicted spot sizes indicate that γ_n's exist that result in a small value of E. These γ_n's tend to minimize the discontinuities of $\phi_H(x, y)$.

6. FOURIER-TRANSFORM LENS

In this section we describe the use of our technique to design an optimum aspheric Fourier-transform lens. We compare the resulting system performance with that obtained from (1) a conventional holographic Fourier-transform lens recorded with spherical wave fronts and (2) an aspheric HOE, both designed with a holographic ray-tracing computer program in conjunction with optimization routines.

Consider the geometry shown in Fig. 1. An input plane is located 0.5 m from a flat, aspheric HOE. The input plane is tilted 20° relative to the HOE. A transparency at the input plane 25.4 mm on each side is illuminated by a coherent plane wave front ($\lambda = 0.5145$ μm). The input transparency produces an angular spectrum of plane wave fronts (one for each spatial-frequency component of the input) that propagate to the HOE. We would like the HOE to focus each incident plane wave front to a corresponding point in the output plane. The output plane is parallel to the HOE and a distance $F =$ 0.5 m away. Furthermore, we would like the location of the points in the outplane to be given by

$$x'' = \lambda F f_{x'}, \quad (27a)$$

$$y'' = \lambda F f_{y'}, \quad (27b)$$

where $f_{x'}$ and $f_{y'}$ are the x and y spatial frequencies, respectively (relative to the input plane), of the corresponding incident plane wave fronts. Equations (27a) and (27b) specify the output-point locations that would result when an ideal Fourier-transform lens is used. The HOE is assumed to be thin and consequently exhibits no volume Bragg effects. Thus the intensity of any point in the output plane depends

Table 1. Input Field Angles (α_l, β_l), Corresponding Spatial-Frequency Components ($f_{x',l}, f_{y',l}$), and Corresponding Nominal Output-Spot Locations for (a) Ideal Fourier-Transform HOE, (b) Conventional Fourier-Transform HOE, and (c) Fairchild–Fienup Aspheric Fourier-Transform HOE

					(a) Ideal Spot Location		(b) Conventional HOE Spot Location		(c) Fairchild–Fienup Aspheric HOE Spot Location	
l	α_l	β_l	$f_{x',l}$ (lines/min)	$f_{y',l}$ (lines/mm)	x'' (mm)	y'' (mm)	x'' (mm)	y'' (mm)	x'' (mm)	y'' (mm)
1	−2.4°	0°	−81.39	0	−20.93783	0.00000	−19.8463	0.00000	−19.8287	0.00000
2	−1.2°	0°	−40.70	0	−10.47121	0.00000	−9.87993	0.00000	−9.8764	0.00000
3	0°	0°	0	0	0.00000	0.00000	0.00000	0.00000	0.00000	0.00000
4	1.2°	0°	40.70	0	10.47121	0.00000	9.80504	0.00000	9.8014	0.00000
5	2.4°	0°	81.39	0	20.93783	0.00000	19.5483	0.00000	19.5291	0.00000
6	0°	−2.4°	0	−81.39	0.00000	−20.93783	0.15001	−20.9562	0.1500	−20.9396
7	0°	−1.2°	0	−40.70	0.00000	−10.97121	0.0375	−10.4735	0.0375	−10.4686
8	0°	1.2°	0	40.70	0.00000	10.47121	0.0375	10.4735	0.0375	10.4686
9	0°	2.4°	0	81.39	0.00000	20.93783	0.15001	−20.9562	0.1500	20.9396

only on the intensity of the corresponding input plane wave.[11] No effort is made to guarantee that the phase difference between two points in the output plane is the same as the phase difference between the two corresponding plane waves diffracted from the input transparency. Thus we are attempting to design a HOE that can be used optically to determine the Fourier spectrum of an input transparency.

Using the technique outlined in Section 4, we determined the optimum aspheric HOE, i.e., $\phi_H(x, y)$, based on nine different input-plane-wave components. If we write the normalized propagation vector $\hat{K}_l$ of the lth plane-wave component relative to the input plane as

$$\hat{K}_l = (\sin \alpha_l)\hat{x}' + (\sin \beta_l)(\cos \alpha_l)\hat{y}' + (\cos \beta_l)(\cos \alpha_l)\hat{z}', \tag{28}$$

where $\hat{x}'$, $\hat{y}'$, and $\hat{z}'$ are the unit vectors along the x', y', and z' axes, respectively, then the corresponding x and y spatial frequencies, $f_{x',l}$ and $f_{y',l}$, respectively, are

$$f_{x',l} = (\sin \alpha_l)/\lambda, \tag{29a}$$

$$f_{y',l} = (\sin \beta_l)(\cos \alpha_l)/\lambda. \tag{29b}$$

Note that α_l and β_l are the x and y propagation angles of the lth plane-wave component with respect to the input aperture. The nine different input-plane-wave components used are given in Table 1. Since input transparencies will, in general, have x and y spatial-frequency components that are simultaneously nonzero, a better choice of input components would be the 17 shown in Fig. 2. However, for comparison purposes, these nine components were chosen to be consistent with those used by Fairchild and Fienup[5] in an earlier design effort. The total area illuminated on the HOE of Fig. 2 by the nine input-plane-wave components of Table 1 is shown in Fig. 3. Columns a of Table 1 are the corresponding ideal point positions in the output plane as given by Eqs. (27a) and (27b). The performance of the aspheric HOE was evaluated by tracing for each α_l and β_l a hexapolar array of 36 rays, with propagation direction $\hat{K}_l$, from the input plane to the output plane. The 36 rays originated from points in the input plane that were spaced as shown in Fig. 4. Figure 5(a) shows the resulting spot diagrams at the output plane for the optimum aspheric HOE. Note that these spot diagrams are derived by ray tracing and consequently do not include boundary diffraction effects. Since the system is symmetric in the β angular direction, we only show spot diagrams for the negative values of β. Each spot diagram shows the relative position of each of the 36 ray intercepts at the output plane. If the system were ideal, all 36 rays would intersect the output plane at a single point. Many of the intercepts shown in Fig. 5(a) are so close together in relation to the scale of the plot that they cannot be individually resolved.

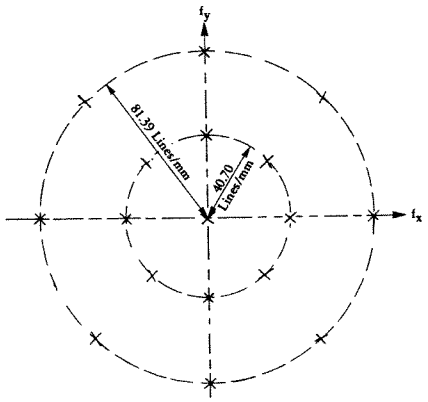

Fig. 2. Locations of 17 plane-wave spatial-frequency components that could be used in the optimization of a practical Fourier-transform HOE.

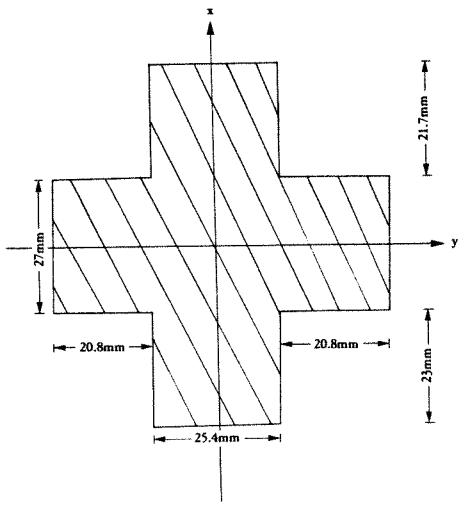

Fig. 3. Region illuminated on the Fourier-transform HOE of Fig. 2 for the nine input-plane components given in Table 1.

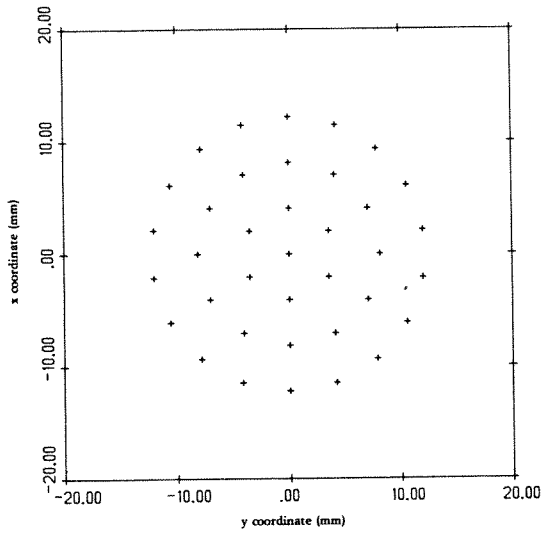

Fig. 4. Locations of the 36 rays at the input plane that are used to compute the output-spot diagrams.

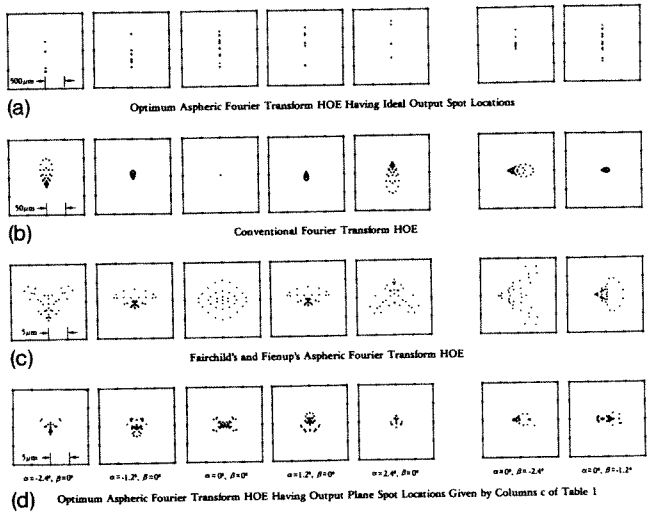

Fig. 5. Spot diagrams predicted by ray tracing (note the different scales for the different cases).

Next consider the conventional holographic Fourier-transform lens produced by two spherical recording beams,[5] as shown in Fig. 6. The performance of this conventional holographic Fourier-transform lens was evaluated as before. The resulting spot diagrams are shown in Fig. 5(b). For each α_l and β_l, columns b in Table 1 give the (x, y) intercept in the output plane of the ray originating from the $x = 0, y = 0$ point in the input plane. The surprising result seen by comparing the spot diagrams in Figs. 5(a) and 5(b) is that the conventional HOE appears to outperform the optimum aspheric HOE. But one has to be careful in interpreting these results since in some sense we are comparing two different systems. This becomes readily apparent when columns a and b of Table 1 are examined. We see that, although the conventional HOE has a smaller spot size than the optimum aspheric HOE at the nine input spatial frequencies, the locations of the spots in the output plane for the conventional HOE system are in the wrong positions. For example, the nominal spot position in the output plane for the conventional HOE system and an input spatial frequency of $f_x = -81.39$ lines/mm, $f_y = 0$ lines/mm is, by columns b of Table 1, $x = -19.8463$ mm, $y = 0.00000$ mm. But by columns a of Table 1 the desired location is -20.93783, $y = 0.0$ mm; thus the nominal spot location in the output plane is off by more than a millimeter.

Here we see that, if we force the spots to be in the proper locations for the optimum HOE, the spot sizes become very large; significant reduction of the spot sizes is possible if one allows distortion to exist.

The rms wave-front error E with respect to the output-spot locations as given by columns b of Table 1 was computed for the conventional HOE using the HOAD ray-trace program. The results are shown in column a of Table 2. The error was computed based on an input-ray distribution of two crossed orthogonal fans of 11 points each, as shown in Fig. 7. Although the wave-front error computed by the HOAD program using these two orthogonal fans is not exactly the quantity E given by Eqs. (15) and (16), it is close.

We examined the performance of an aspheric HOE designed with the aid of a holographic ray-tracing computer program in conjunction with optimization routines. This design work was performed by Fairchild and Fienup[6] for the basic system configuration shown in Fig. 1. Their recording-beam geometry was that of Fig. 6, except that Fairchild and Fienup allowed the plane reference-beam wave front to be perturbed by the phase function

$$\frac{2\pi}{\lambda}(C_{20}x^2 + C_{40}x^4 + C_{60}x^6 + C_{80}x^8 + C_{02}y^2 + C_{04}y^4 + C_{06}y^6 + C_{08}y^8 + C_{22}x^2y^2 + C_{44}x^4y^4),$$

where x and y refer to the coordinate system in the plane of the HOE. All 10 of the C_{ij} coefficients were allowed to vary during a damped-least-squares optimization. The merit function consisted of the sum of the squares of the rms spot size at the output plane for the nine spatial frequencies given earlier. The spot positions were not optimized, i.e., distortion was ignored. The resulting spot diagrams, calculated as before, are shown in Fig. 5(c). For each α_l and β_l, columns c of Table 1 give the (x, y) intercept in the output plane of the ray originating from the $x = 0, y = 0$ point in the input plane. Notice the geometric distortion of the image by comparing columns c and a of Table 1. Also notice that the nominal spot positions are roughly the same as those of the conventional HOE system (compare columns c and b of Table 1).

By choosing the desired output-spot locations to be the same as the nominal output-spot locations as given by columns

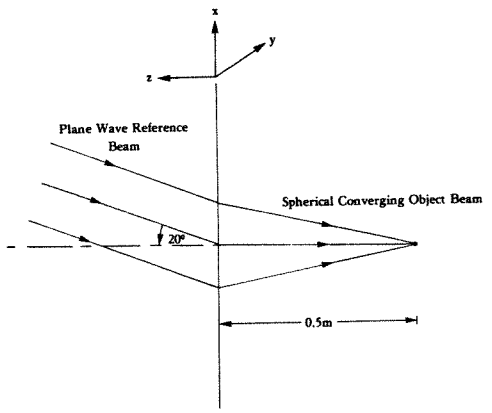

Fig. 6. Construction geometry for conventional Fourier-transform HOE.

Table 2. Input Field Angle (α_l, β_l) and Corresponding Approximate rms Wave-Front Error E_l for (a) Conventional Fourier-Transform HOE, (b) the Fairchild–Fienup Aspheric Fourier-Transform HOE, (c) Optimum Aspheric Fourier Transform HOE

l	α_l	β_l	(a) Conventional HOE [$\sim E_l$ (in wavelengths)]	(b) Fairchild–Fienup Aspheric HOE [$\sim E_l$ (in wavelengths)]	(c) Optimum Aspheric HOE [$\sim E_l$ (in wavelengths)]
1	−2.4°	0°	2.75×10^{-1}	3.72×10^{-2}	3.95×10^{-2}
2	−1.2°	0°	0.84×10^{-1}	2.55×10^{-2}	2.75×10^{-2}
3	0°	0°	0	3.85×10^{-2}	2.52×10^{-2}
4	1.2°	0°	0.89×10^{-1}	2.48×10^{-2}	2.76×10^{-2}
5	2.4°	0°	3.07×10^{-1}	3.88×10^{-2}	3.99×10^{-2}
6	0°	−2.4°	2.33×10^{-1}	4.59×10^{-2}	5.59×10^{-2}
7	0°	−1.2°	0.71×10^{-1}	2.68×10^{-2}	4.00×10^{-2}
8	0°	1.2°	0.71×10^{-1}	2.68×10^{-2}	4.05×10^{-2}
9	0°	2.4°	2.33×10^{-1}	4.59×10^{-2}	5.59×10^{-2}
			$E = 1.84 \times 10^{-1}$ [a]	$E = 3.54 \times 10^{-2}$ [a]	$E = 4.06 \times 10^{-2}$ [a]

[a] $E = \left[\frac{1}{9}\sum_{l=1}^{9} E_l^2\right]^{1/2}$.

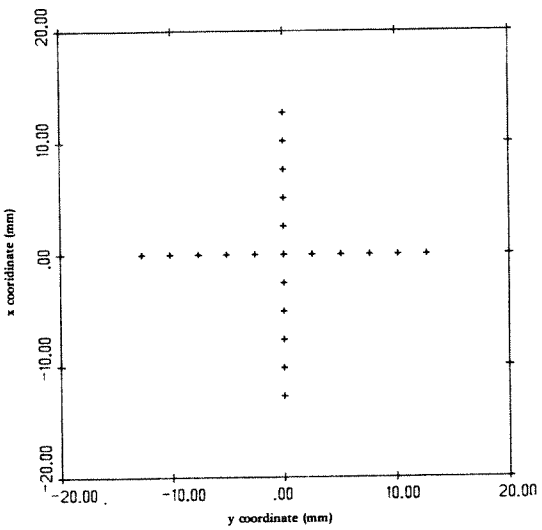

Fig. 7. Locations of the 21 rays at the input plane that were used to compute the rms wave-front error.

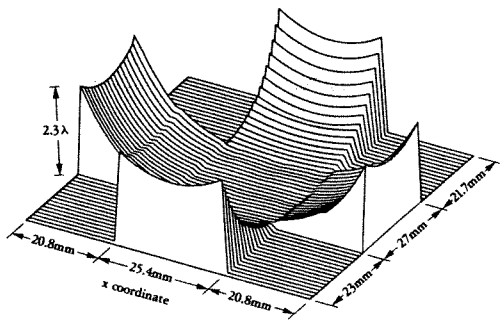

Fig. 8. Reference-beam phase perturbation required to produce the optimum Fourier-transform HOE.

c of Table 1, the wave-front error of this HOE was computed by the HOAD program, and the results are shown in column b of Table 2. From both Table 2 and Fig. 5 it can be seen that the Fairchild–Fienup design is several times better than the conventional HOE.

The optimum aspheric HOE corresponding to the output-plane spot locations given by column c of Table 1 [rather than those given by Eqs. (27a) and (27b)] was determined. This allowed us to compare the optimum aspheric HOE with the HOE designed by Fairchild and Fienup. However, in order to avoid the considerable computation associated with calculating the a_i's and b_{jk}'s of Eq. (23) by numerical integration, we used the following simpler approach. Since for this problem the ray-trace-predicted spot sizes are small, there must exist γ_n's that yield a small rms wave-front error E, as discussed earlier. These γ_n's will tend to minimize the magnitude of the discontinuities of the $\phi_H(x, y)$. Using formula (26) and the relation $\gamma_l - \gamma_m = c_{lm}$, it was easy to find γ_n's that resulted in discontinuities of relatively small magnitudes. These γ_n's were used in Eq. (19) to compute the phase transfer function $\phi_H(x, y)$. Thus the "optimum" aspheric HOE actually was not optimum since the γ_n's as given by Eq. (23) were not used to compute $\phi_H(x, y)$. For this reason the rms wave-front error, given in column c of Table 2, was actually a little worse than that of the design of Fairchild and Fienup. However, as can be seen from the spot diagrams in Fig. 5(d), the geometric spot sizes, which are independent of the γ_n's, are considerably better than those for the design of Fairchild and Fienup.

From Eq. (2) it is seen that only the difference between the object- and reference-beam phases determines $\phi_H(x, y)$. Therefore $\phi_{\text{obj}}(x, y)$ can be chosen arbitrarily, and then Eq. (2) determines $\phi_{\text{ref}}(x, y)$. $\phi_{\text{obj}}(x, y)$ was chosen to correspond to a spherical wave front converging to the point $x = 0, y = 0$ in the output plane, i.e.,

$$\phi_{\text{obj}}(x, y) = -\frac{2\pi}{\lambda}[x^2 + y^2 + (0.5)^2]^{1/2}. \tag{30}$$

By combining Eqs. (2), (19), and (30), ϕ_{ref} can then be expressed as

$$\phi_{\text{ref}}(x, y) = -\frac{2\pi}{\lambda} x[\sin(20°)] + \phi_{\text{pert}}(x, y), \tag{31}$$

where the phase function $\phi_{\text{pert}}(x, y)$, the perturbation of ϕ_{ref} from a tilted plane wave, is shown in Fig. 8. Therefore this HOE can be recorded by using the setup shown in Fig. 6, provided that the phase perturbation shown in Fig. 8 is added to the plane reference-beam wave front by using a computer-generated hologram.

7. ADDITIONAL COMMENTS

In this paper we have shown how to determine the phase transfer function $\phi_H(x, y)$ of a flat aspheric HOE to minimize the mean-squared wave-front error of the element averaged over some finite set of input wave fronts. It should be noted that this optimum phase transfer function, which is explicitly given by Eq. (19), is discontinuous. The transfer function would be continuous, however, if the $P_n(x, y)$'s were tapered to be continuous. This is an area of research that should be pursued.

A consideration that has not been discussed in this paper is that of realizability. It has not been shown that, in general, there will exist propagating object- and reference-beam wave fronts that will interfere to produce the desired hologram phase transfer function [see Eq. (2)]. This was not a problem for the simple Fourier-transform lens that we analyzed and should not be a problem for the HOE's having small numerical apertures.

Another area that has not been explored is that of Bragg efficiency in thick HOE's. Since only the difference between the object- and reference-beam phases affects $\phi_H(x, y)$, there will be an infinite number of combinations of object and reference beams that yield the desired transfer function. From among these, one should choose the combination that most nearly satisfies the Bragg condition for all the input wave fronts. This will ensure the highest possible diffraction efficiency for the element.

Every optical imaging element, whether it be conventional or holographic, will exhibit to some degree the five basic monochromatic third-order aberrations—spherical aberration, coma, astigmatism, field curvature, and distortion.[10] The spherical aberration, coma, astigmatism, and field curvature degrade the image by increasing the impulse-response spot size. By using our technique, the total mean-squared wave-front error, including distortion, is minimized. In the examples described in Section 6, it was seen that it may be impossible to achieve low values for all five of the monochromatic aberrations at once. However, by specifying the desired output-point locations so that these locations are somewhat distorted from those desired, the resulting optimum aspheric HOE had greatly reduced values of the other aberrations. Thus there is a trade-off between distortion and the other aberrations. This trade-off can be clearly seen by writing the desired phase $\phi_n(x, y)$ of the nth output wave front as $\phi_n(x, y; \bar{r}_n)$, where $\bar{r}_n$ is the (x, y, z) coordinate of the corresponding image point. Thus $\phi_{H,n}(x, y)$ [see Eq. (5)] is now written as $\phi_{H,n}(x, y; \bar{r}_n)$. Allowing for optimization over spot positions in the same way that we previously allowed for optimization over the γ_n's, Eq. (15) and (20) become

$$E^2 \triangleq \eta \min G(\gamma_1, \gamma_2, \ldots, \gamma_N; \bar{r}_1, \bar{r}_2, \ldots, \bar{r}_N) \quad (32)$$

and

$$G(\gamma_1, \gamma_2, \ldots, \gamma_N, \bar{r}_1, \bar{r}_2, \ldots, \bar{r}_N) = \sum_{n=1}^{N} W_n \iint P_n(x, y) \left(\left[\sum_{m=1}^{N} W_m P_m(x, y) \right]^{-1} \times \left\{ \sum_{m=1}^{N} W_m P_m(x, y) [\phi_{H,m}(x, y; \bar{r}_m) - \gamma_m] \right\} - [\phi_{H,n}(x, y; \bar{r}_n) - \gamma_n] \right)^2 dx\,dy. \quad (33)$$

Clearly, there will be some choice of $\bar{r}_1, \bar{r}_2, \ldots, \bar{r}_N$ that minimizes G and consequently minimizes the rms wave-front error E. We note, however that $\bar{r}_1, \bar{r}_2, \ldots, \bar{r}_N$ directly determine the field curvature and distortion of the HOE. Furthermore, the $\bar{r}_1, \bar{r}_2, \ldots, \bar{r}_N$ that minimizes E, and as a result minimizes the observed spot size, will not, in general, minimize the distortion and field curvature.

It is often possible to determine approximately the $\bar{r}_1, \bar{r}_2, \ldots, \bar{r}_N$ that minimizes the output-spot sizes. A procedure for doing so is outlined below along with its heuristic justification. It is assumed that there exist some $\bar{r}_1, \bar{r}_2, \ldots, \bar{r}_N$ such that the output-spot sizes are small. Choose some region on the HOE where a large number of input wave-fronts overlap. For the HOE to perform perfectly in this overlap region, a different phase transfer function $\phi_{H,n}(x, y)$ would be required for each of the input wave fronts. Thus, if the HOE is to perform well over this overlap region, the different phase transfer functions must be approximately the same to within an additive constant, i.e., there must exist $\bar{r}_1, \bar{r}_2, \ldots, \bar{r}_N$ such that

$$\phi_{H,j}(x, y; \bar{r}_j) \simeq \phi_{H,k}(x, y; \bar{r}_k) + c_{jk}, \quad (34)$$

where c_{jk} is an arbitrary constant for all pairs of input wave fronts j and k within the overlap region. Pick one of the input wave fronts in this overlap region (assumed to be the mth) and choose $\bar{r}_m$ to be the desired output image location for that input wave front. From formulas (5) and (34), we want to find the $\bar{r}_k$'s corresponding to the remaining wave fronts in the overlap region such that

$$\phi_{k,\text{out}}(x, y; \bar{r}_k) \simeq \phi_{k,\text{in}}(x, y) + \phi_{H,m}(x, y; \bar{r}_m) + c_{km}. \quad (35)$$

Formula (35) indicates that $\bar{r}_k$ is the coordinates of the point focus formed by ray tracing the kth input wave front through a hologram in the overlap region formed by the mth input wave front and the corresponding desired mth output wave front. The above procedure can be repeated in different overlap regions until all the remaining $\bar{r}_k$'s are determined.

As an example, consider the Fourier-transform lens design of Section 6. The overlap region is taken to be some small neighborhood about $x = 0, y = 0$. All the input wave fronts do not overlap in this region, but for simplicity we will assume that they do. Choose $m = 3$ (i.e., $\alpha = 0°, \beta = 0°$), and for each input wave front trace the ray to the output plane that goes through the point $x = 0, y = 0$ on the HOE. The coordinates of the intercepts of these rays on the output plane are given by columns b of Table 1. Note from columns c of Table 1 that these intercepts agree quite well with the $\bar{r}_k$'s used in the Fairchild–Fienup design and in our optimum design.

The paraxial approximation might also be used to handle the $\bar{r}_k$'s. With this approximation, the effect of changing $\bar{r}_k = (x_k, y_k, z_k)$ is expressed analytically by adding to $\phi_{H,k}(x, y)$ phase terms proportional to $x_k x$ and $y_k y$ for wave-front tilt and $z_k(x^2 + y^2)$ for focusing. The total wave-front error could then possibly be minimized over the parameters x_k, y_k, and z_k in a manner similar to that used for the γ_k's.

8. SUMMARY

In this paper, we have studied the problem of designing a thin, flat aspheric holographic optical element that will image a finite set of input wave fronts into a finite set of output wave

fronts. We have analytically determined the phase transfer function of the HOE that is optimum. By optimum, we mean that such an element has minimum mean-squared wave-front error averaged over the set of input wave fronts.

It was shown that it is not always possible to obtain a low value for the mean-squared wave-front error. For the Fourier-transform element that we studied, low values for spherical aberration, coma, and astigmatism may be obtained by permitting distortion. Our analysis indicates that a previous computer-optimization technique for designing aspheric HOE's achieved low values for spherical aberration, coma, and astigmatism only because it permitted distortion.

The power and the generality of computer-optimization methods make it unlikely that these methods will ever be completely replaced by analytic design techniques, such as those described in this paper. Analytic techniques, however, allow the designer to obtain a physical understanding of the design process, and they may aid him in achieving superior designs.

As was noted in the introduction, conventional lenses cannot be exactly described by a phase transfer function, and so the design approach described here is not immediately applicable to them. However, with appropriate modifications, weighted sums of optimal surfaces (or of approximate phase transfer functions) could possibly be useful for conventional lenses.

APPENDIX A

$$
\begin{aligned}
&G(\gamma_1, \gamma_2, \ldots, \gamma_N) \\
&= \iint \Bigg(\sum_{n=1}^{N} W_n P_n(x,y) \\
&\quad \times [\phi_{H,n}(x,y) - \gamma_n]^2 - \left[\sum_{s=1}^{N} W_s P_s(x,y) \right]^{-1} \\
&\quad \times \left\{ \sum_{r=1}^{N} W_r P_r(x,y) [\phi_{H,r}(x,y) - \gamma_r] \right\}^2 \Bigg) \mathrm{d}x\mathrm{d}y, \qquad \text{(A1)} \\
&= \iint \Bigg\{ \sum_{n=1}^{N} W_n P_n(x,y) \\
&\quad \times [\phi_{H,n}{}^2(x,y) - 2\phi_{H,n}(x,y)\gamma_n + \gamma_n{}^2] \\
&\quad - \left[\sum_{s=1}^{N} W_s P_s(x,y) \right]^{-1} \sum_{r=1}^{N} \sum_{t=1}^{N} W_r P_r(x,y) W_t P_t(x,y) \\
&\quad \times [\phi_{H,r}(r,y)\phi_{H,t}(x,y) - \phi_{H,r}(x,y)\gamma_t \\
&\quad - \phi_{H,t}(x,y)\gamma_r + \gamma_r \gamma_t] \Bigg\} \mathrm{d}x\mathrm{d}y, \qquad \text{(A2)} \\
&= \text{const.} + \sum_{n=1}^{N} a_n \gamma_n + \sum_{j=1}^{N} \sum_{k=1}^{N} b_{jk} \gamma_j \gamma_k, \qquad \text{(A3)}
\end{aligned}
$$

where

$$
\begin{aligned}
\text{const.} = \iint \Bigg\{ & \sum_{n=1}^{N} W_n P_n(x,y) \phi_{H,n}{}^2(x,y) \\
& - \left[\sum_{s=1}^{N} W_s P_s(x,y) \right]^{-1} \sum_{r=1}^{N} \sum_{t=1}^{N} W_r P_r(x,y) \\
& \times W_t P_t(x,y) [\phi_{H,r}(x,y)\phi_{H,t}(x,y)] \Bigg\} \mathrm{d}x\mathrm{d}y, \qquad \text{(A4)}
\end{aligned}
$$

$$
\begin{aligned}
a_n = & -2W_n \iint P_n(x,y)\phi_{H,n}(x,y)\mathrm{d}x\mathrm{d}y \\
& + 2W_n \iint \left[\sum_{s=1}^{N} W_s P_s(x,y) \right]^{-1} P_n(x,y) \\
& \times \left[\sum_{m=1}^{N} W_m P_m(x,y)\phi_{H,m}(x,y) \right] \mathrm{d}x\mathrm{d}y, \qquad \text{(A5)}
\end{aligned}
$$

and

$$
\begin{aligned}
b_{jk} = & \delta_{jk} W_j \iint P_j(x,y)\mathrm{d}x\mathrm{d}y \\
& - W_j W_k \iint \left[\sum_{s=1}^{N} W_s P_s(x,y) \right]^{-1} \\
& \times P_j(x,y) P_k(x,y)\mathrm{d}x\mathrm{d}y, \qquad \text{(A6)}
\end{aligned}
$$

where δ_{jk} is the Kronecker delta function

$$
\delta_{jk} = \begin{cases} 1, & j = k \\ 0, & j \neq k \end{cases}. \qquad \text{(A7)}
$$

Note that, from Eq. (A6), $b_{jk} = b_{kj}$.

ACKNOWLEDGMENTS

We thank T. R. Crimmins for providing the assertions made in this paper following Eqs. (22) and (23). This research was supported by the U.S. Air Force Wright Aeronautical Laboratories under contract F33615-80-C-1077.

* Present address, Lincoln Laboratory, Massachusetts Institute of Technology, P.O. Box 73, Lexington, Massachusetts 02173.

REFERENCES

1. D. H. Close, "Holographic optical elements," Opt. Eng. **14**, 408–419 (1975).
2. W. H. Lee, "Computer-generated holograms: techniques and applications," in *Progress in Optics*, E. Wolf, ed. (Wiley, New York, 1978), Vol. 16.
3. J. W. Goodman, *Introduction to Fourier Optics* (McGraw-Hill, New York, 1968).
4. E. B. Champagne, "Nonparaxial imaging, magnification, and aberration properties in holography," J. Opt. Soc. Am. **57**, 51–55 (1967); "A qualitative and quantitative study of holographic imaging, Ph.D. dissertation, Ohio State University, Columbus, Ohio (1967).
5. J. R. Fienup and C. D. Leonard, "Holographic optics for a matched filter optical processor," Appl. Opt. **18**, 631–640 (1979).
6. R. C. Fairchild and J. R. Fienup, "Computer-originated hologram lenses," Opt. Eng. **21**, 133–140 (1982).
7. J. N. Latta and R. C. Fairchild, "New developments in the design of holographic optics," Proc. Soc. Photo-Opt. Instrum. Eng. **39**, 107–126 (1973).
8. J. N. Latta, "Computer-based analysis of holography using ray tracing," Appl. Opt. **10**, 2698–2710 (1971).
9. D. Feder, "Automatic optical design," Appl. Opt. **2**, 1209–1226 (1963).
10. M. Born and E. Wolf, *Principles of Optics* (Pergamon, New York, 1975).
11. R. Collier, C. Burkhardt, and L. Lin, *Optical Holography* (Academic, New York, 1971), Chaps. 8 and 9.